A Coupled Extended-Finite-Discrete Element Method: On the Different Contact Schemes between Continua and Discontinua

Shervin Khazaeli, Shahab Haj-zamani

Abstract—Recently, advanced geotechnical engineering problems related to soil movement, particle loss, and modeling of local failure (i.e. discontinua) as well as modeling the in-contact structures (i.e. continua) are of the great interest among researchers. The aim of this research is to meet the requirements with respect to the modeling of the above-mentioned two different domains simultaneously. To this end, a coupled numerical method is introduced based on Discrete Element Method (DEM) and eXtended-Finite Element Method (X-FEM). In the coupled procedure, DEM is employed to capture the interactions and relative movements of soil particles as discontinua, while X-FEM is utilized to model in-contact structures as continua, which may consist of different types of discontinuities. For verification purposes, the new coupled approach is utilized to examine benchmark problems including different contacts between/within continua and discontinua. Results are validated by comparison with those of existing analytical and numerical solutions. This study proves that extended-finite-discrete element method can be used to robustly analyze not only contact problems, but also other types of discontinuities in continua such as (i) crack formations and propagations, (ii) voids and bimaterial interfaces, and (iii) combination of previous cases. In essence, the proposed method can be used vastly in advanced soil-structure interaction problems to investigate the micro and macro behaviour of the surrounding soil and the response of the embedded structure that contains discontinuities.

Keywords—Contact problems, discrete element method, extended-finite element method, soil-structure interaction.

I. Introduction

IN numerical modeling of physical phenomena, using the proper approach is the key factor to reach the realiable and realistic results. The true granular nature of the soil implies that we need to utilize discrete elements (DE) in order to capture macro/micro-scale behaviour, [1] and [2]. On the other hand, in many cases they can be in contact with structures, which are continues media. In such cases, utilizing the conventional finite elements (FE) is promising to model the continuum. Therefore, the coupled finite-discrete element can befit from the advantages of both approaches [3]. As the result, a wide spectrum of dynamic problems related to geotechnical engineering and in the context of soil-structure interaction (SSI) can be treated in different scales [4]-[9]. Moreover, a combined finite-discrete element method [5] allows DEs to be meshed and treated as deformable media. However, with the existence of discontinuities in the continua, a wide variety of problems cannot be investigated effectively by FEM with respect to computational costs because it requires remeshing and employing mesh adaptivity techniques as time evolves [4].

Different types of discontinuities may exist or appear in a continues medium, especially in SSI problems such as analyzing crack propagations in (semi)-buried structures, debonding in multi-materials, the damage analysis of the avalanche on the roads and so on. The reader is referred to [4], [7], and [8] for a complete study of different interaction problems between continua and discontinua. Generally, two types of discontinuity may be examined within a physical modeling, namely weak and strong discontinuity. Briefly, in the former one, the solution (displacement) field continues, while the gradients (strain and stresses) experience a jump. Bimaterial and inclusions are of this type of discontinuity. On the other hand, the latter type of discontinuity is associated with a jump in both solution and its gradients such as crack propagation and contacts. X-FEM is a relatively new and robust approach in order to model discontinuities in continua [4]. In this method, the problem domain is independent of the generated mesh by introducing proper additional functions into the solution of the governing equation (i.e. enriched functions). In fact, the nature of the discontinuity is captured in the solution field in contrast with the conventional FEM in which the discontinuity is directly defined within meshing procedure. Choosing the additional functions depends on the phenomena under consideration. In another words, based on the behaviour of the discontinuity, it is required to chose functions with the same behaviour. As a result, introducing a new framework based on coupling of X-FE and DE methods allow us to model more complex systems including discontinua and discontinuities within discontinua.

In the following study, the governing equations of both DEM and X-FEM are presented and discretized. Then, the coupling procedure based on X-FE and DE methods (X-FE-DEM) is introduced to trace the interaction between two media. The main focus here is to address three different types of contact including (a) contact between particles in discontinua, (b) contact between two different continua, and (c) contact between discontinua and continua. The DEM accounts for the interaction and relative movement of soil particles as discontinuum at both microscale and macroscale levels (Type a). The unpredictable location and direction of the movements of granular materials make DEM a promising approach for analyzing these types of problems. With the aid of proper enriched functions, X-FEM is able to model

S. Khazaeli is PhD student at Concordia University, Montreal, QC, Canada (e-mail: s_khaz@encs.concordia.ca).

S. Haj-zamani is M.Eng student at McGill University, Montreal, QC, Canada (e-mail: shahab.haj-zamani@mail.mcgill.ca).

structures including different types of discontinuities. In such a model, the selection of the enriched functions is conducted based on the phenomenon under consideration. Here, the aim is to model discontinuities in which the displacement in the medium changes rapidly (i.e. strong discontinuity). This rapid change is due to different continua that are in contact with each other (Type b). As mentioned, by applying X-FEM, complications related to meshing of the continuum are eliminated and computational costs decreased significantly. Moreover, the interchange of the induced forces between two (DE and X-FE) domains is carried out carefully by introducing interface elements at the boundary of the continua and discontinua (Type c). Finally, proper numerical scheme for explicit and implicit approaches (see Appendices B and C) are employed to solve and compare the results of some basic problems based on FE-DEM and X-FE-DEM.

II. Problem Statement

Consider the problem of a continuum defined in domain Ω with boundaries Γ_u, Γ_t, and Γ_c, which are displacement, traction, and inner contact boundary conditions. Moreover, the continuum is in contact with a discontinum, defined in domain Ω^*, along the boundary Γ_t^*. The superscript "$*$" emphasis on the fact that the latter medium discontinues so the interaction and the subsequent force transfer between two media occurred at finite points, $\boldsymbol{x}^p$. The strong form of the problem related to

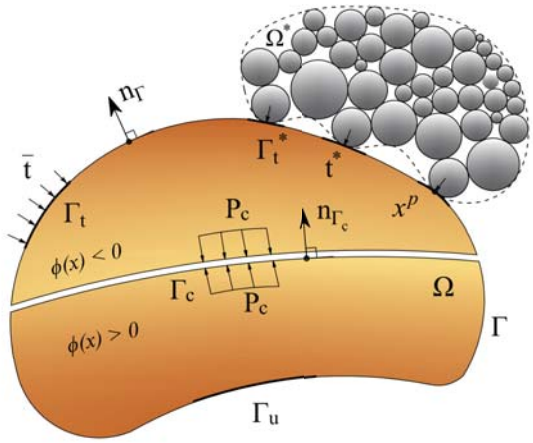

Fig. 1 The interaction of in-contact continua with discontinuum

the continuum can be written as:

$$\begin{aligned} \nabla.\boldsymbol{\sigma} - \rho\ddot{\mathbf{u}} + \rho\mathbf{b} &= \mathbf{0}, && \text{in } \Omega \\ \boldsymbol{\sigma} &= \mathbf{D}\boldsymbol{\epsilon}, && \text{in } \Omega \\ \boldsymbol{\epsilon} &= \nabla^s\mathbf{u}, && \text{in } \Omega \end{aligned} \tag{1}$$

with the boundary and initial conditions

$$\begin{aligned} \boldsymbol{\sigma}.\mathbf{n} &= \bar{\mathbf{t}}, && \text{on } \Gamma_t \\ \boldsymbol{\sigma}.\mathbf{n} &= \mathbf{t}^*, && \text{on } \Gamma_d^* \\ \boldsymbol{\sigma}.\mathbf{n} &= \mathbf{p_c}, && \text{on } \Gamma_c \\ \mathbf{u} &= \bar{\mathbf{u}}, && \text{on } \Gamma_u \\ \mathbf{u} &= \mathbf{u}_0, && \text{at } t = 0 \\ \dot{\mathbf{u}} &= \dot{\mathbf{u}}_0. && \text{at } t = 0 \end{aligned} \tag{2}$$

In (1) and (2), ∇ is the Nabla operator and ∇^s is expressed as $\nabla^s = \frac{1}{2}\left(\nabla^T + \nabla\right)$. In addition, $\boldsymbol{\sigma}$ is the Cauchy stress tensor, ϵ is the strain tensor, ρ is the density, $\mathbf{b}$ is the body force vector, $\mathbf{D}$ is the elasticity constitutive tensor, $\mathbf{u}$ is the displacement field, the upper dot(s) denotes the derivative(s) with respect to time, $\mathbf{n}$ represents the outward normal on the continuum, and $\bar{\mathbf{t}}$ and $\bar{\mathbf{u}}$ are prescribed traction and displacement along the boundary. Moreover, $\mathbf{t}^*$ and $\mathbf{p_c}$ are transferred forces between two media and the contact force within the continuum, respectively. The proposed governing equation is discretized within the forthcoming sections and implemented to solve the interaction problem. In addition, the governing translational and rotational equations corresponding to each particle i of the discontinuum may be written as:

$$\begin{aligned} \mathbf{m}_i\ddot{\mathbf{r}}_i &= \mathbf{F}_i, && \text{in } \Omega^* \\ \mathbf{I}_i\dot{\boldsymbol{\omega}}_i &= \mathbf{M}_i. && \text{in } \Omega^* \end{aligned} \tag{3}$$

In which $\mathbf{m}_i$ is the mass vector, $\mathbf{r}_i$ is the position vector, $\mathbf{I}_i$ is the inertia vector, $\boldsymbol{\omega_i}$ is the angular velocity, and $\mathbf{F}_i$ and $\mathbf{M}_i$ are the transferred force and moments to the particle. In the coupled method, equations sets (1) and (3) must be solved simultaneously. To this end, the next sections are casting to discretizing the equations and coupling them together in order to solve the interaction problem. It is notable that the radiation condition also must be satisfied.

III. Governing Discretized Equation

A. DE Framework

In this framework, the state of the particles (discontinua) are determined by utilizing the discrete (distinct) element approach. Based on an explicit scheme, the translational and rotational accelerations of the particles with respect to time are obtained by knowing the total force (torque) and the particles' inertia, [9] and [10]. In the absence of rotational effects the governing differential equations of the particle i can be determined by the first equation of (3) as:

$$\mathbf{m}_i\frac{d^2}{dt^2}\mathbf{r}_i = \mathbf{F}_i. \tag{4}$$

In the study of granular materials, out-of-balance force transfer includes deformation of the particles at contact points. However, to model the contact, certain stiffness are defined and converted to the external forces through the overlapping of in-contact particles. As the result, in the absence of capillary, fluid and external specified forces, the total force vector may be written as [7]

$$\mathbf{F}_i = \sum_{j\neq i}\mathbf{F}_{ij}^c + \mathbf{F}_i^g. \tag{5}$$

Here, $\mathbf{F}_i^g$ is the gravitational force and $\mathbf{F}_{ij}^c$ is the transmitting contact force to the particle i through the set of other particles that are in contact [11].

$$\mathbf{F}_{ij}^c = \begin{cases} 0 & , \Delta_{ij}^n > 0 \\ -K_{ij}^n\Delta_{ij}^n - \eta^n\frac{d}{dt}\Delta_{ij}^n & , \Delta_{ij}^n < 0, \end{cases} \tag{6}$$

in which η^n is a viscous damping constant and Δ_{ij}^n is the normal overlap of the two particles calculated as:

$$\Delta_{ij}^n = \frac{d_{ij}}{2} - \bar{r}_{ij}, \qquad \bar{r}_{ij} = \frac{r_i + r_j}{2}, \tag{7}$$

where r_i and r_j are the radii of in-contact spheres and $d_{ij}$is the distance between the centers of the two spheres. Moreover, K_{ij}^n is the normal stiffness between two particles:

$$\frac{1}{K_{ij}^n} = \bar{r}_{ij}\left(\frac{1}{k_i^n} + \frac{1}{k_j^n}\right), \tag{8}$$

where k_i^n is the stiffness of each particle. It is worth noting that in this study the effect of normal contact is considered and the reader is referred to [7] and [11] for sliding and rolling contact.

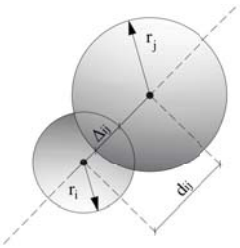

Fig. 2 The contact model between two particles

B. X-FE Framework

In order to analyze the continuum region of the problem the so-called X-FEM is utilized. In this framework additional (enriched) functions are applied to the approximated solution of the discretized governing equation in the conventional finite element method [4].

$$\mathbf{u}(\boldsymbol{x}, t) = \mathbf{N}^{std}(\boldsymbol{x})\,\bar{\mathbf{u}}(t) + \mathbf{N}^{enr}(\boldsymbol{x})\,\bar{\mathbf{a}}(t) \tag{9}$$

In (9), the first and second terms are referred to standard and enriched parts of the solution, $\mathbf{N}^{std}(\boldsymbol{x})$ are the standard shape functions, $\mathbf{N}^{enr}(\boldsymbol{x})$ are the enriched functions, and $\bar{\mathbf{u}}(t)$ and $\bar{\mathbf{a}}(t)$ are the unknown solution vectors at time t corresponding to standard and enriched terms of the approximation field, respectively. The characteristics of the enriched functions should coincide with the phenomena under consideration. Here, the focus is on the contact problem; therefore, it is required to select a function which shows the discontinuity or jump on both solution field and its corresponding gradients, displacement and strain, respectively. To capture the kinematics of this type of jump, known as strong discontinuity, the Heaviside (step) function can be employed [12]. For the ith node, the corresponding enriched shape function can be calculated as

$$N_i^{enr} = N_i^{std}(x)\left[H(\phi(x)) - H(\phi(x_j))\right]. \tag{10}$$

in which,

$$H(\phi(x)) = \begin{cases} +1 & \phi(x) \geq 0 \\ 0 & \phi(x) < 0. \end{cases}, \tag{11}$$

where $\phi(x)$ is the signed distance function, which is used to locate the discontinuity interface [4]. To model the frictionless contact, the penalty method is utilized in which the contact constrains are defined by certain stiffness at the interface between two bodies, $\mathbf{K}_{\text{con}}$ (see Appendix.A). As here we develop and investigate the normal contacts, the corresponding elasto-plastic modulus tensor in contact stiffness reduces to normal stiffness k_n (penalty constant). Interestingly, while in DEM framework the effect of penetration is introduced as an external forces on other particles, in X-FE framework the normal contact effects between two continuua are introduced as a stiffness directly into the global stiffness matrix. The discretized X-FEM equation can be written as [12] and [13]

$$\mathbf{M}\ddot{\bar{\mathbf{U}}} + \mathbf{K}\bar{\mathbf{U}} - \mathbf{f}^{\text{ext}} = \mathbf{0} \tag{12}$$

in which $\mathbf{M}$, and $\mathbf{K}$ are the mass and stiffness matrices of the continuum, $\mathbf{f}^{\text{ext}}$ is the external force vector, and $\bar{\mathbf{U}} = \langle \bar{\mathbf{u}}, \bar{\mathbf{a}} \rangle$ is the vector of standard and enriched degrees of freedom. The details of (12) are presented in Appendix A.

IV. Coupled X-FE-DEM

In the coupled method, (1) and (3) must be solved at the same time. A modified flowchart [10], Fig. 3, is proposed, which is composed of three main fusions, namely initiation, interaction, and solver fusion. The term "fusion" is used to emphasize on the fact that at each stage two different media must be simultaneously analyzed.

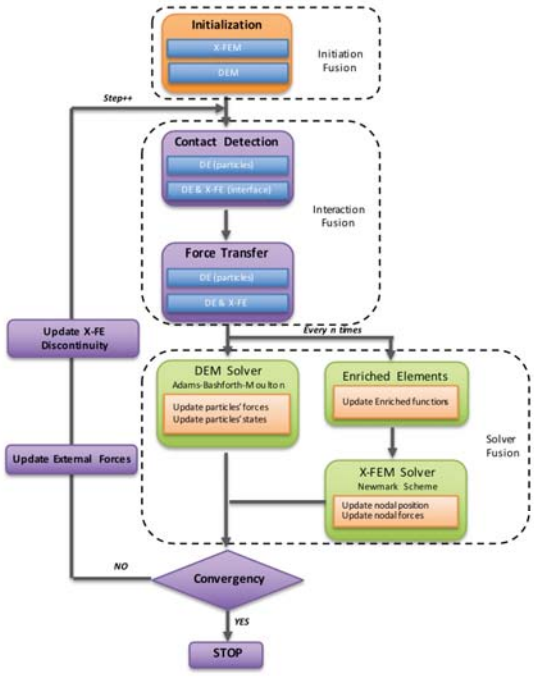

Fig. 3 The solution procedure of X-FE-DEM

In initiation fusion, the geometry and material properties of both domains and discontinuities are defined. The interaction fusion consists of detecting contact between discontinua and continua as well as interchanging forces between them. In the last fusion, the governing equations associated with each medium are solved with a step-delay of n [14]. In another

words, for every n-step time evolution of the discontinua, the state of the continuum is updated. Choosing the proper value of n is crucial for the stability of the procedure [14]. In this work, the n is set to 10. Moreover, it is worth noting that in this study the primary concern is to investigate the normal contact phenomenon between different types of elements. Here, specific enriched shape function is used, which is not changed during the solution of the problem. However, different enriched functions can be utilized during the solution procedure depends on different physical phenomena such as changing the mode of the crack in analyzing the crack propagation problems.

A. Contacts

Based on Fig. 1, three different contacts are determined; contact between particles of discontinua (Type a), contact between two continua along the contact interface (Type b), and contact between discontinua and continua (Type c). For Type a, contact traction boundary condition method [7] is utilized in which the interacting forces are added to the external force vector of the bodies. In conventional FEM, the contact problem is treated by the interface element method introduced at the contact zone. However, in X-FEM the Type b contact is modeled independent of FE mesh and the solution fields of those elements which are cut by the contact interface are approximated by additional specific enriched shape functions. In two dimensional problems, the contact of the particles and discontinua can be appeared in two cases; edge and vertex collisions. In both cases the traction boundary condition method is used in such a way that in the former case all the forces are transmitted into the corresponding node, while in latter one the applied forces are distributed between two adjacent vertices. Fig. 4 depicts the two different collisions in Type c contact.

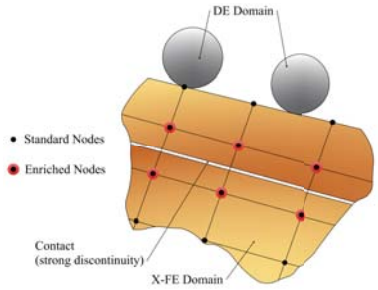

Fig. 4 Type c contacts between the continuum and discontinuum

B. Interface Element

In order to properly treat the coupled method, an interface element is defined to obtain geometrical parameters and force distribution [14]. In this study, the interface element is a segment with two nodes numbered 0 and 1 as shown in Fig. 5. These two nodes can be enriched depending on the location of the contact interface.

Based on Kuhn-Tucker rule, the contact condition between the particles and the continuum is addressed when the following relationship for the normal gap function g_n is hold:

$$g_n = \left(\boldsymbol{x}^{(c)} - \boldsymbol{x}^{(p)}\right).\mathbf{n}_{\Gamma_t^*} \leq R. \tag{13}$$

where $\boldsymbol{x}^{(c)}$ and $\boldsymbol{x}^{(p)}$ are the coordinates of particle center and the contact point, respectively and R is the particle radius. The contact normal $\mathbf{n}_{\Gamma_c}$ and contact point $\boldsymbol{x}^{(p)}$ are expressed as [9] and [13]:

$$\mathbf{n}_{\Gamma_t^*} = \frac{\boldsymbol{x}^{(c)} - \boldsymbol{x}^{(p)}}{\left|\left|\boldsymbol{x}^{(c)} - \boldsymbol{x}^{(p)}\right|\right|} \tag{14}$$

$$\boldsymbol{x}^{(p)} = \frac{\boldsymbol{x}^{(1)} + \boldsymbol{x}^{(c)}.\left(\boldsymbol{x}^{(1)} - \boldsymbol{x}^{(0)}\right) - \boldsymbol{x}^{(0)}.\left(\boldsymbol{x}^{(1)} - \boldsymbol{x}^{(0)}\right)}{\left|\left|\boldsymbol{x}^{(1)} - \boldsymbol{x}^{(0)}\right|\right|^2} \tag{15}$$

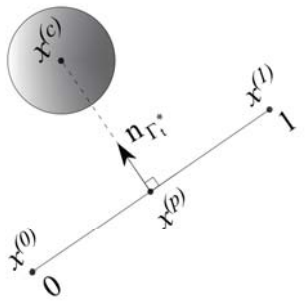

Fig. 5 Interface element

It is worth noting that if the following relationship is hold, one may conclude that the particle is in contact at the edge, otherwise, it is considered as node collision [13]:

$$\delta < \frac{\left(\boldsymbol{x}^{(p)} - \boldsymbol{x}^{(0)}\right).\left(\boldsymbol{x}^{(1)} - \boldsymbol{x}^{(0)}\right)}{\left|\left|\boldsymbol{x}^{(1)} - \boldsymbol{x}^{(0)}\right|\right|^2} < 1 - \delta, \tag{16}$$

in which δ is a small value close to zero. Finally, the induced force due to the particle i on the adjacent nodes can be evaluated as

$$\mathbf{f}^c = \left(\mathbf{N}^{enh}\right)^T \mathbf{F}^{d-c}, \tag{17}$$

where $\mathbf{N}^{enh} = \langle \mathbf{N}^{std}, \mathbf{N}^{enr} \rangle$ and the superscript $d-c$ denotes the force transfer between dicontinua and continua

$$\mathbf{F}^{d-c} = \begin{cases} 0 & , r_i - g_n > 0 \\ k_i^n \left(r_i - g_n\right) & , r_i - g_n < 0, \end{cases} \tag{18}$$

C. DEM Time Step Equation

Equation (4) is a second-order differential equation, which can be converted into the two first-order differential equation. So, for the ith particle one may obtain

$$\begin{aligned} \frac{d}{dt}\mathbf{r}_i &= \mathbf{v}_i, \\ \frac{d}{dt}\mathbf{v}_i &= \mathbf{F}_i/\mathbf{m}_i. \end{aligned} \tag{19}$$

The Adams-Bashforth-Moulton multi-step method [15], [16] can be utilized to evaluate the system of equations of the form $\frac{d}{dt}\mathbf{y} = \mathbf{f}(\mathbf{y}, t)$ such that the position of particles at the unknown time step $n+1$ is predicted explicitly, $\mathbf{y}^*$ and corrected implicitly, $\mathbf{y}$ by means of (20).

$$\mathbf{y}^{*}\left(t_{n+1}\right)=\mathbf{y}\left(t_{n}\right)+\Delta t^{DEM}.\mathbf{f}\left(\mathbf{y}\left(t_{n}\right),t_{n}\right)$$
$$\mathbf{y}\left(t_{n+1}\right)=\mathbf{y}\left(t_{n}\right)+\Delta t^{DEM}.\mathbf{f}\left(\mathbf{y}^{*}\left(t_{n+1}\right),t_{n+1}\right) \quad (20)$$

in which $\Delta t^{DEM}=t_{n+1}^{DEM}-t_{n}^{DEM}$. In order to assure the stability of DEM, the critical time step Δt_{cr} can be determined

$$\Delta t_{cr}^{DEM}=\min\sqrt{\frac{2m_i}{K_i}}. \quad (21)$$

It is worth noting that although the presented method takes the advantages of both explicit and implicit formulations, one may consider it as an explicit method as the corrected state of the particle $\mathbf{y}\left(t_{n+1}\right)$ in left-hand-side of (20) is obtained by using the predicted state at of the particle in right-hand side of the equation (i.e. $\mathbf{f}\left(\mathbf{y}^{*}\left(t_{n+1}\right),t_{n+1}\right)$). Moreover, as the predictor-corrector procedure utilizes the previous three solution points, for the first three steps the 4th order Runge-Kutta method may be employed. A brief algorithm of the solution procedure is provided in Algorithm 2.

D. X-FEM Time Step Equation

For the continuum region of the problem, generalized Newmark GN_{22} scheme is used in order to discretized the time domain of the governing equation.

$$\begin{aligned}\ddot{\bar{\mathbf{U}}}_{n+1}&=\frac{1}{\beta\Delta t^{2}}\left(\bar{\mathbf{U}}_{n+1}-\bar{\mathbf{U}}_{n}\right)\\&\quad-\frac{1}{\beta\Delta t}\dot{\bar{\mathbf{U}}}_{n}-\left(\frac{1}{2\beta}-1\right)\ddot{\bar{\mathbf{U}}}_{n},\\\dot{\bar{\mathbf{U}}}_{n+1}&=\frac{\gamma}{\beta\Delta t}\left(\bar{\mathbf{U}}_{n+1}-\bar{\mathbf{U}}_{n}\right)\\&\quad-\left(\frac{\gamma}{\beta}-1\right)\dot{\bar{\mathbf{U}}}_{n}-\Delta t\left(\frac{\gamma}{2\beta}-1\right)\ddot{\bar{\mathbf{U}}}_{n},\end{aligned} \quad (22)$$

where $(\beta,\gamma)\in[0,1]$ are Newmark parameters, which it is required to satisfy $\gamma\geq 0.5,\beta\geq 0.25\left(\gamma+0.5\right)^{2}$ in order to unconditionally stabilize the time integration procedure. For the sake of simplicity and unless otherwise mentioned, Δt without superscript is corresponding to X-FEM time step. Finally, by substituting (22) in (12), one can obtain the following non-linear equation that may be linearized and evaluated by means of Newton-Raphson itterative algorithm. The procedure of the algorithm is provided briefly in Appendix B.

$$\mathbf{M}\ddot{\bar{\mathbf{U}}}_{n+1}+\mathbf{K}\bar{\mathbf{U}}_{n+1}-\mathbf{G}_{\mathbf{U}_{n+1}}=\mathbf{0}, \quad (23)$$

where $\mathbf{G}_{\mathbf{U}_{n+1}}$ is a known vector obtained from previous time step t_n.

$$\begin{aligned}\mathbf{G}_{\mathbf{U}_{n+1}}=\mathbf{f}_{\mathbf{U}_{n+1}}^{\mathrm{ext}}+\mathbf{M}&\left(\frac{1}{\beta\Delta t^{2}}\bar{\mathbf{U}}_{n}+\frac{1}{\beta\Delta t}\dot{\bar{\mathbf{U}}}_{n}\right.\\&\left.+\left(\frac{1}{2\beta}-1\right)\ddot{\bar{\mathbf{U}}}_{n}\right).\end{aligned} \quad (24)$$

V. Validation

In this section, some problems are solved in order to verify the proposed method. In the first problem the effect of normal contact stiffness on the over-lapping of the a particle is investigated. Then, the Newmark scheme for the conventional FEM and X-FEM is examined on an axial bar under the an external time vary force. Afterwards, the coupled FE-DEM and X-FE-DEM are compared under the external force due to collision of particle(s).

Consider a spherical shape with a unit mass and the normal stiffness k. In the first problem, the mass is released from a height of $3m$ into the ground which is fixed. Collisions happen through time as shown in Fig. 6 based on Adams-Bashforth-Moulton scheme. In this figure, the effect of normal stiffness is investigated. As it is seen, the overlap is reduced as the contact stiffness is increased. It is notable that the damping coefficient is calculated as $\eta^{n}=0.2\sqrt{m_i/k_i}$.

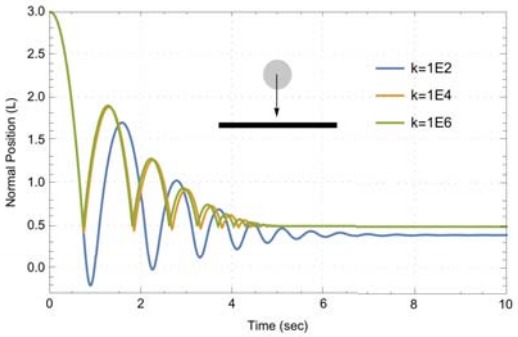

Fig. 6 The effect of normal contact stiffness on the collision trajectory based on Adams-Bashforth-Moulton scheme

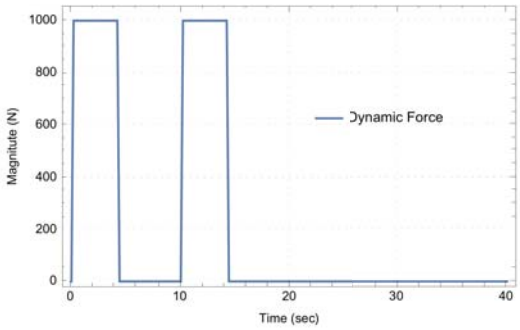

Fig. 7 External dynamic load

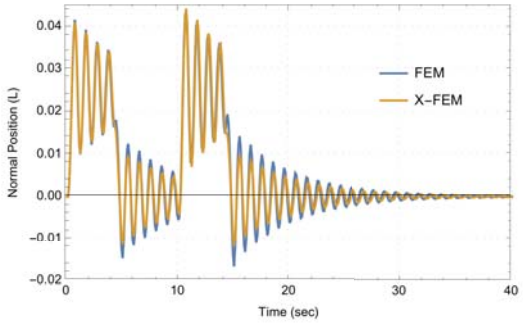

Fig. 8 The response of the system based on Newmark scheme due to the external dynamic loading

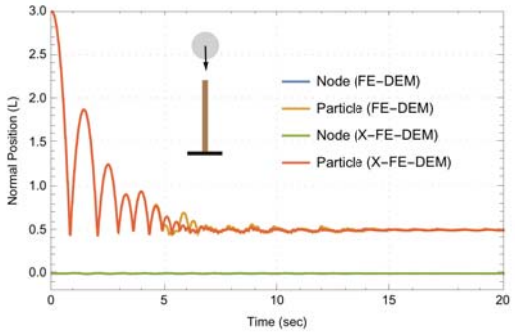

Fig. 9 Comparison between FE-DEM and X-FE-DEM for case I

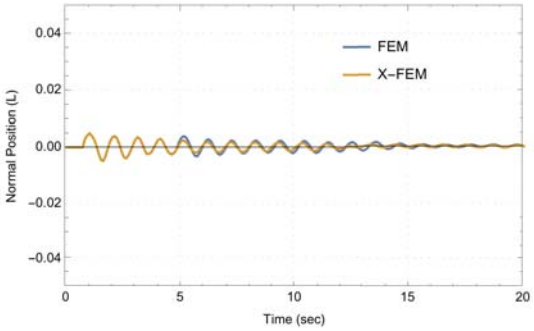

Fig. 10 Comparison between the response of the continua in FE-DEM and X-FE-DEM for case I

For the next problem, the Newmark scheme is applied to solve the problem of an axial rod exposed to a dynamic force as shown in Fig. 7. The rod has a modulus of elasticity of $E = 3e7$, cross section of $A = 0.4$, density of $\rho = 2000$ and the height of $L = 30m$. It is worth noting that the Newmark parameters $\beta = 0.4$ and $\gamma = 0.6$ and the penalty factor is assumed $100E$. Fig. 8 depicts the response of the free node at the end of the rod under above-mentioned loading. As it is seen, both FEM and X-FEM are in good agreement. Figs. 9 and 10 illustrate the response of the system due to interaction with one particle, $Case\ I$, in both FEM and X-FEM framework. In Fig. 9, the emphasis is on the trajectory of the particle in both approaches. It is evident that after many collisions and damping, the relative movement of the particle tends to zero. Moreover, Fig. 10 shows the response of the free end-node for a selected period of time in order to show the accuracy of the X-FE-DEM method. In the last problem, the system is excited by means of two particles, $Case\ II$. All three types of normal contacts are involved in the problem. Figs. 11 and 12 show the solution of the system by virtue of FE-DEM and X-FE-DEM, respectively. In addition, Figs. 13 and 14 take a closer look at each response corresponding to the continua and discontinua and make a comparison between FE-DEM and X-FE-DEM. It is depicted that both methods coincide with each other with a good approximation. However, as mentioned before, X-FE-DEM has advantages with respect to mesh independency, which allows us to model different types of discontinuities. It is worth noting that after a certain time, (approximately 20 sec), the relative movement of the system tends to be zero due to the radiation condition.

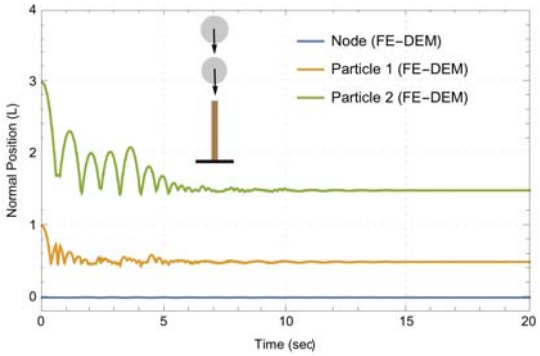

Fig. 11 FE-DEM modeling of the system in case II

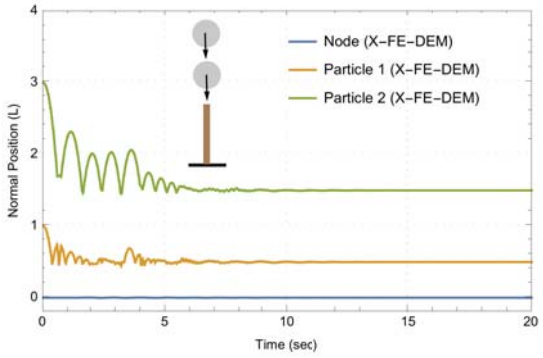

Fig. 12 X-FE-DEM modeling of the system in case II

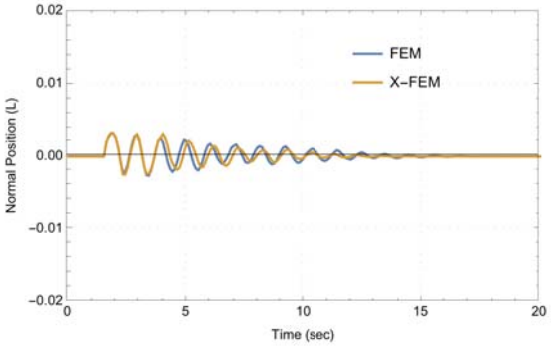

Fig. 13 Comparison between the response of the continua in FE-DEM and X-FE-DEM for case II

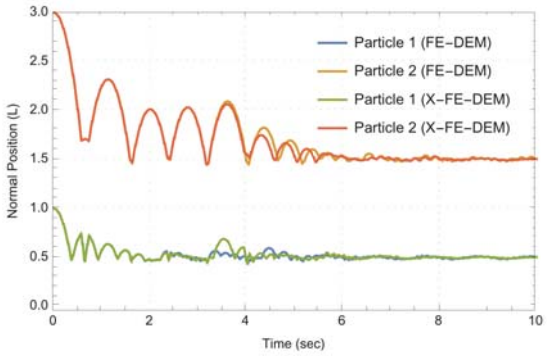

Fig. 14 Comparison between the response of the discontinua in FE-DEM and X-FE-DEM for case II

VI. Conclusion

In this study, a coupled numerical method is introduced based on DEM and X-FEM. The presented approach (X-FE-DEM) has the capability of modelling continua and discontinua, simultaneously. Moreover, due to mesh independency of the X-FEM, modelling of different type of strong and weak discontinuities are carried with a computational cost efficiency. Here, the focus is on the different normal contacts between media. Three main contacts are determined within continua and discontinua as well as between them. Two main examples in one dimension are solved and the results are compared with of those from the conventional FE-DEM. It is found that the results are in a very good agreement with each other. As the result, by extending the examples into the two and three dimension, real complex geotechnical problems especially in SSIs can be treated with more efficiency with respect to both accuracy and computational costs. Moreover, due to flexibility of the X-FEM other types of discontinuities such as bi-material, crack propagation, and so on can be investigated thoroughly for large-scale geotechnical problems.

Appendix A
X-FEM Discritization Equation

The discretized equation of (12) can be written as:

$$\begin{pmatrix} \mathbf{M}_{uu} & \mathbf{M}_{ua} \\ \mathbf{M}_{au} & \mathbf{M}_{aa} \end{pmatrix} \begin{Bmatrix} \ddot{\bar{\mathbf{u}}} \\ \ddot{\bar{\mathbf{a}}} \end{Bmatrix} + \begin{pmatrix} \mathbf{K}_{uu} & \mathbf{K}_{ua} \\ \mathbf{K}_{au} & \mathbf{K}_{aa} + \mathbf{K}_{\text{con}} \end{pmatrix} \begin{Bmatrix} \bar{\mathbf{u}} \\ \bar{\mathbf{a}} \end{Bmatrix} - \begin{Bmatrix} \mathbf{f}_u^{\text{ext}} \\ \mathbf{f}_a^{\text{ext}} \end{Bmatrix} = \mathbf{0}, \tag{25}$$

where

$$\begin{aligned} \mathbf{M}_{\alpha\beta} &= \int_\Omega (\mathbf{N}^\alpha)^T \rho\, \mathbf{N}^\beta d\Omega \\ \mathbf{K}_{\alpha\beta} &= \int_\Omega (\mathbf{B}^\alpha)^T \mathbf{D}\, \mathbf{B}^\beta d\Omega \\ \mathbf{K}_{\text{con}} &= \int_{\Gamma_c} \left(\mathbf{N}^{std}\right)^T \mathbf{D}^{ep}\, \mathbf{N}^{std} d\Gamma \\ \mathbf{f}_\alpha^{\text{ext}} &= \int_\Omega (\mathbf{N}^\alpha)^T \rho\, d\Omega + \int_{\Gamma_t} (\mathbf{N}^\alpha)^T \bar{\mathbf{t}}\, d\Gamma \\ &\quad + \sum_{\Gamma_t^*} (\mathbf{N}^\alpha)^T \mathbf{F}^{d-c}, \end{aligned} \tag{26}$$

in which $(\alpha, \beta) \in (std, enr)$ represent the standard and enriched parts and $\mathbf{D}^{ep}$ is elasto-plastic modulus tensor in contact stiffness $\mathbf{K}_{\text{con}}$.

Appendix B
Newmark Scheme Algorithm

The Newmark scheme algorithm for implicitly solve the dynamic equation of (12) is shown in the following algorithm.

Algorithm 1: Newmark scheme for solving dynamic equation implicitly

Initialization
Claculate $\mathbf{K}_0$, $\mathbf{A}_0$, $\mathbf{A}_1$, $\mathbf{A}_2$
Set $\bar{\mathbf{U}}_0, \dot{\bar{\mathbf{U}}}_0, \ddot{\bar{\mathbf{U}}}_0$ | initial conditions
foreach *time step,* $n = 0, 1, \ldots$ **do**
  $\bar{\mathbf{U}}_{n+1}^0 = \bar{\mathbf{U}}_n$
  $\Delta\bar{\mathbf{U}}_{n+1}^0 = \mathbf{0}$
  for *iteration,* $i = 0, 1, \ldots$ **do**
    $\bar{\mathbf{U}}_{n+1}^{i+1} = \bar{\mathbf{U}}_{n+1}^i + \Delta\bar{\mathbf{U}}_{n+1}^i$
    Newmark Scheme:
      Calculate $\dot{\bar{\mathbf{U}}}_{n+1}^{i+1}, \ddot{\bar{\mathbf{U}}}_{n+1}^{i+1}$ | $\bar{\mathbf{U}}_{n+1}^{i+1}, \bar{\mathbf{U}}_n, \dot{\bar{\mathbf{U}}}_n, \ddot{\bar{\mathbf{U}}}_n$
    Calculate $\mathbf{J}^{i+1}$
    Calculate $\mathcal{R}\bar{\mathbf{U}}_{n+1}^{i+1}$
    if *convergence* **then**
      Break
    end
    $\Delta\bar{\mathbf{U}}_{n+1}^{i+1} = -\left(\mathbf{J}^{i+1}\right)^{-1} \mathcal{R}\bar{\mathbf{U}}_{n+1}^{i+1}$
  end
end

In above algorithm $\mathcal{R}\bar{\mathbf{U}}_{n+1}$ is the residual vector corresponding to Eq.23, which may be written as:

$$\begin{aligned} \mathcal{R}\bar{\mathbf{U}}_{n+1} &= \mathbf{K}_0\bar{\mathbf{U}}_{n+1} - \mathbf{F}_{n+1}^{ext} \\ &\quad - \mathbf{A}_0\bar{\mathbf{U}}_n - \mathbf{A}_1\dot{\bar{\mathbf{U}}}_n - \mathbf{A}_2\ddot{\bar{\mathbf{U}}}_n, \end{aligned} \tag{27}$$

in which

$$\begin{aligned}
\mathbf{K}_0 &= -\frac{\gamma}{\beta\Delta t}\left(\frac{1}{\beta\Delta t^2}\mathbf{M}+\mathbf{K}\right)\\
\mathbf{F}_{n+1}^{ext} &= -\frac{\gamma}{\beta\Delta t}\mathbf{f}_{\mathbf{U}_{n+1}}^{\text{ext}}\\
\mathbf{A}_0 &= -\frac{\gamma}{\beta\Delta t}\left(\frac{1}{\beta\Delta t^2}\mathbf{M}\right)\\
\mathbf{A}_1 &= -\frac{\gamma}{\beta\Delta t}\left(\frac{1}{\beta\Delta t}\mathbf{M}\right)\\
\mathbf{A}_2 &= -\frac{\gamma}{\beta\Delta t}\left(\left(\frac{1}{2\beta}-1\right)\mathbf{M}\right),
\end{aligned} \tag{28}$$

and the Jacobian matrix $\mathbf{J}=\mathbf{K}_0$

APPENDIX C
ADAMS-BASHFORTH-MOULTON ALGORITHM

In order to explicitly find the solution of (20), a two step algorithm can be employed as shown here.

Algorithm 2: Adams-Bashforth-Moulton scheme for solving dynamic equation explicitly

Initialization
Set $\mathbf{y}(t_0)$ | initial condition
Runge-Kutta scheme:
Calculate $\mathbf{y}(t_1)$, $\mathbf{y}(t_2)$, $\mathbf{y}(t_3)$:
$\mathbf{y}(t_{n+1}) = \mathbf{y}(t_n) + \frac{\Delta t}{6}(\mathbf{S}_1 + 2\mathbf{S}_2 + 2\mathbf{S}_3 + \mathbf{S}_4)$
foreach *time step,* $n = 3, 4, ...$ **do**
Adams-Bashforth-Moulton scheme:
Calculate (predict):

$$\begin{aligned}
\mathbf{y}^*(t_{n+1}) =& \mathbf{y}(t_n) + \frac{\Delta t}{24}[55\mathbf{f}(\mathbf{y}(t_n), t_n)\\
&- 59\mathbf{f}(\mathbf{y}(t_{n-1}), t_{n-1})\\
&+ 37\mathbf{f}(\mathbf{y}(t_{n-2}), t_{n-2})\\
&- 9\mathbf{f}(\mathbf{y}(t_{n-3}), t_{n-3})]
\end{aligned} \tag{29}$$

Calculate (correct):

$$\begin{aligned}
\mathbf{y}(t_{n+1}) =& \mathbf{y}(t_n) + \frac{\Delta t}{24}[9\mathbf{f}(\mathbf{y}^*(t_{n+1}), t_{n+1})\\
&+ 19\mathbf{f}(\mathbf{y}(t_n), t_n)\\
&- 5\mathbf{f}(\mathbf{y}(t_{n-1}), t_{n-1})\\
&+ \mathbf{f}(\mathbf{y}(t_{n-2}), t_{n-2})]
\end{aligned} \tag{30}$$

end

in above algorithm, $\mathbf{S}_i$ are expressed as

$$\begin{aligned}
\mathbf{S}_1 &= \mathbf{f}(\mathbf{y}(t_n), t_n)\\
\mathbf{S}_2 &= \mathbf{f}\left(\mathbf{y}(t_n) + \mathbf{S}_1\frac{\Delta t}{2}, t_n + \frac{\Delta t}{2}\right)\\
\mathbf{S}_3 &= \mathbf{f}\left(\mathbf{y}(t_n) + \mathbf{S}_1\frac{\Delta t}{2}, t_n + \frac{\Delta t}{2}\right)\\
\mathbf{S}_4 &= \mathbf{f}(\mathbf{y}(t_n) + \mathbf{S}_3\Delta t, t_n + \Delta t)
\end{aligned} \tag{31}$$

ACKNOWLEDGMENT

The authors would like to fully acknowledge the Department of Civil, Building, and Environmental Engineering of Concordia university and the Department of Mining and Materials Engineering of McGill University, Montral, Canada as well as their faculties for the support provided to accomplish this work. Moreover, we would like to thank the recent graduate student, Ali Salehi, the University of British Columbia, Vancouver, Canada for reviewing the manuscript and helping with the preparation of illustrations and figures.

REFERENCES

[1] L. Jing and O. Stephansson, *Fundamentals of discrete element method for rock engineering: Theory and applications*, Elsevier, Amsterdam, Netherlands, 2007.
[2] F. V. Donz, V. Richefeu and S. A. Magnier, *Advances in discrete element method applied to soil, rock and concrete mechanics*, State of the art of geotechnical engineering. Electronic Journal of Geotechnical Engineering, 44, 31., 2009
[3] E. Onate, J. Rojeck, *Combination of discrete element and finite element methods for dynamic analysis of geomechanics problems*, Computer Methods in Applied Mechanics and Engineering, 193(27):30873128, 2004.
[4] A. R. Khoei, *Extended finite element method: Theory and applications*, John Wiley and Sons, West Sussex, 2014.
[5] A. Munjiza, *The Combined Finite-Discrete Element Method*, John Wiley and Sons, West Sussex, 2004.
[6] W. Xu, M. Zang, W. Gao *Adaptive combined DE/FE algorithm for brittle fracture of plane stress problems*, Computational Mechanics, 54(2):535546, 2014.
[7] C. OSullivan, *Particulate discrete element modelling: A geomechanics perspective*, Spon Press., 2011.
[8] S. Mohammadi, *XFEM Fracture Analysis of Composites*, John Wiley and Sons, West Sussex, 2012.
[9] H. k. Dang and M. A. Meguid, *An efficient finitediscrete element method for quasi-static nonlinear soilstructure interaction problems*, International Journal for Numerical and Analytical Methods in Geomechanics, 37(2), 130-149. doi:10.1002/nag.1089, 2013.
[10] V. Tran, *A coupled finite-discrete element framework for soil-structure interaction analysis*, PhD thesis, Department of Civil Engineering and Applied Mechanics, McGill University, Montreal, Canada, 2013.
[11] H. G. Matuttis and J. Chen, *Understanding the discrete element method: Simulation of non-spherical particles for granular and multi-body systems*, John Wiley and Sons (Asia) Pte., 2014.
[12] A. R. Khoei, M. Vahab, *A numerical contact algorithm in saturated porous media with the extended finite element method*, International Journal of Computational Mechanics 54:10891110, 2014.
[13] H. Chen, X. Y. Zhang, M. Zang, and P. L. Hazell, *An accurate and robust contact detection algorithm for particle-solid interaction in combined finite-discrete element analysis*, International Journal for Numerical Methods in Engineering, 103(8), 598-624. doi:10.1002/nme.4913, 2015.
[14] V. Tran, M. A. Meguid, and L. Chouinard *Three-dimensional analysis of geogrid-reinforced soil using a finite-discrete element framework*, International Journal of Geomechanics. DOI: 10.1061/(ASCE)GM.1943-5622.0000410, 2014.
[15] J. C. Butcher, *Numerical methods for ordinary differential equations in the 20th century*, Journal of Vomputational and Applied Mathematics, 125: 1-29, 2000.
[16] J. C. Butcher, and G. Wanner, *Runge-Kutta methods: some historical notes*, Journal of Applied Numerical Mathematics, 22: 113-151, 1996.